

# Comparative evaluation of isogeometric analysis and classical FEM with regard to contact analysis

Zishan Naveed<sup>1</sup>, Arnold Kühhorn<sup>1</sup>, Markus Kober<sup>1</sup>

<sup>1</sup>Brandenburg University of Technology (BTU) Cottbus-Senftenberg,  
Chair of Structural Mechanics and Vehicle Vibrations

## Abstract

Isogeometric analysis represents a newly developed technique that offers the application of Computer Aided Design (CAD) concept of Non-uniform Rational B-Splines (NURBS) tool to describe the geometry of the computational domain. The simplified transition of CAD models into the computational domain eliminates the problems arising from the geometrical discontinuities induced by the faceted approximation of the mesh. Moreover, numerical analysis directly on NURBS objects significantly reduces the design-to-analysis time compared to traditional FEA approach. In the field of contact mechanics, when finite elements are applied to geometry with curved surfaces, the result is a non-smooth geometrical representation of interface surfaces which may lead to mesh interlocking, high jumps and spurious oscillations in contact forces. To eliminate these issues, various surface smoothing strategies are to be employed in case of FEM. Isogeometric based analysis alleviates these issues without employing any additional smoothing strategy due to inherent higher order continuity of NURBS basis functions and much more accurate results are obtained compared to conventional FE approach. In the current study, LS-DYNA is used to demonstrate the capabilities and advantage of an isogeometric analysis through an example of pendulum under gravitational load. The numerical simulation results are analytically validated and the comparison of NURBS surfaces with faceted surfaces is carried out to investigate the accuracy.

## 1 Introduction

The main difficulty in contact analysis of cylindrical parts is non-smoothness because traditional finite elements utilize element facets to represent the contact surfaces. The inevitable peaks and valleys on the meshed surfaces of the cylindrical components may inhibit the rotation of these parts when parts are coarsely meshed. Mesh refinement decreases the deviation from the true surface and allows the rotation but high and low spots can never be eliminated from the mesh. The surface normals can undergo jumps across the facet boundaries and may lead to spurious oscillations in contact forces due to the faceted surfaces [1]. This problem becomes more prominent for the case of large sliding contact problems or large curvature surfaces. Various surface smoothing strategies are to be employed to circumvent the geometrical discontinuities by smoothing the surface using spline interpolation. In smooth contact algorithms, an additional smooth curve fitted surface is introduced on top of the existing finite element mesh. This includes an extra layer of data management and increases computational effort [2].

Another remedy to geometric discontinuity is the isogeometric approach, wherein NURBS are utilized for both geometric representation and analysis framework. This approach yields exact shape of geometry even at a coarse discretization. Thus, this approach inherently encounters the issues originated from the finite element approach. Due to these default properties of isogeometric analysis (IGA), it has been highly recommended for the study of contact problems as there is no need for additional smoothing approaches. In this paper, an example of a pendulum and a cylindrical roller bearing are used for the comparative study between classical FEM and IGA.

## 2 Preliminaries

In isogeometric analysis, B-Splines and NURBS basis functions are commonly used for the CAD modeling and discretization of geometries and are defined in the parametric space [3]. A short introduction of these functions is summarized below.

### 2.1 B-splines

B-splines are composed of a linear combination of B-splines basis functions. The vector-valued coefficients of the basis functions are called control points, while the basis functions are constructed by a knot vector. A knot vector  $\xi$  is a non-decreasing set of parametric space coordinates, shown as [3]:

$$\mathcal{E} = \{ \xi_1, \xi_2, \dots, \xi_{n+p+1} \} \quad (1)$$

where each knot entry,  $\xi_i$ , represents a real number (i.e.,  $\xi_i \in \mathbb{R}$ ),  $p$  denotes the order of the B-spline and  $n$  is the total number of B-spline basis functions. A knot vector can be categorized as a uniform or as a non-uniform vector. If the knots are equally spaced, it is called uniform vector, otherwise a non-uniform vector. A knot vector is said to be an open knot vector if the first and last knot value of a knot vector appear  $p+1$  times, which is the standard in CAD literature. B-spline basis functions based on the knot vector  $\mathcal{E}$  and order  $p$ , are obtained from the Cox-de Boor recursion formula [3]:

$$\text{for } p = 0, \quad N_{i,0}(\xi) = \begin{cases} 1, & \text{if } \xi_i \leq \xi < \xi_{i+1}, \\ 0, & \text{Otherwise} \end{cases} \quad (2)$$

$$\text{for } p > 0, \quad N_{i,p}(\xi) = \frac{\xi - \xi_i}{\xi_{i+p} - \xi_i} N_{i,p-1} + \frac{\xi_{i+p+1} - \xi}{\xi_{i+p+1} - \xi_{i+1}} N_{i+1,p-1}.$$

B-spline basis functions are piecewise polynomials and constitute a partition of unity  $\sum_{i=1}^n N_{i,p}(\xi) = 1$  for all  $\xi_1 \leq \xi \leq \xi_{n+p+1}$ . They are pointwise non-negative over the entire domain, i.e.  $N_{i,p}(\xi) \geq 0, \forall \xi$ . Their continuity depends on  $\mathcal{E}$  only. If a knot value is not repeated in the knot vector  $\mathcal{E}$ , then the  $p^{\text{th}}$  order B-spline function  $N_{i,p}(\xi)$  has  $C^{p-1}$  continuity at the knot point. The continuity can also be decreased to  $C^{p-m}$  if a knot has multiplicity  $m$ . In particular, the basis becomes interpolatory at the knot where the multiplicity of the knot is exactly  $p$  because the continuity of the basis becomes  $C^0$  at that knot. Multivariate B-spline basis functions are generated through the tensor product of the univariate basis functions. As an example, the bivariate B-spline basis functions are defined as:

$$N_{i,j}^{p,q}(\xi, \eta) = N_{i,p}(\xi) M_{j,q}(\eta) \quad (3)$$

where  $N_{i,p}$  and  $M_{j,q}$  are  $p^{\text{th}}$  and  $q^{\text{th}}$  order B-spline basis functions that are defined in  $\xi$  and  $\eta$  parametric directions, respectively [4]. Once the B-spline functions are known, a  $p^{\text{th}}$  order B-spline curve can be defined as:

$$C(\xi) = \sum_{i=1}^n N_{i,p}(\xi) B_i \quad (4)$$

where  $B$  represents the array of the control points [3]. For a given control net  $B_{i,j}$ , the B-spline surface is defined through the tensor product of univariate B-spline basis functions as

$$S(\xi, \eta) = \sum_{i=1}^n \sum_{j=1}^m N_{i,p}(\xi) M_{j,q}(\eta) B_{i,j} \quad (5)$$

where  $n$  and  $m$  represent the total number of basis functions defined along the  $\xi$ - and  $\eta$ - parametric directions, respectively.

## 2.2 NURBS

NURBS are frequently employed in CAD industries and are able to accurately represent the complex geometries and conic sections such as circles and ellipses. The NURBS basis is defined as:

$$R_{i,p}(\xi) = \frac{N_{i,p}(\xi) w_i}{W(\xi)} \quad (6)$$

where  $w_i \geq 0$  is referred to as the weight value associated with control point vector  $B_i$  and weighting function  $W(\xi) = \sum_{i=1}^n N_{i,p}(\xi) w_i$  is the weighted linear combination of the standard B-spline basis function [3]. The bivariate NURBS functions are given by:

$$R_{i,j}^{p,q}(\xi, \eta) = R_{i,p}(\xi) R_{j,q}(\eta) = \frac{N_{i,p}(\xi) M_{j,q}(\eta)}{\sum_{i=1}^n \sum_{j=1}^m N_{i,p}(\xi) M_{j,q}(\eta) w_{i,j}} \quad (7)$$

where  $w_{i,j}$  denotes the control point net [3]. NURBS basis functions  $R_{i,p}(\xi)$  in conjunction with control points  $B_i$  define the NURBS curve [3]:

$$C(\xi) = \sum_{i=1}^n R_{i,p}(\xi) B_i. \quad (8)$$

NURBS surfaces are defined through the tensor product of the univariate NURBS basis function according to [3] as:

$$S(\xi, \eta) = \sum_{i=1}^n \sum_{j=1}^m R_{i,j}^{p,q}(\xi, \eta) B_{i,j}. \quad (9)$$

### 3 Pendulum under gravitational load test case

In this section, a pendulum under gravity load, shown in Fig. 1, suspended from the top and swinging freely is investigated.

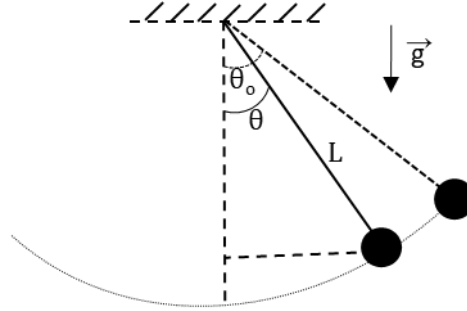


Fig. 1: Schematic diagram of the pendulum.

We assume that the pendulum arm is rigid and massless. Then the constitutive equation governing the pendulum becomes:

$$\frac{d^2\theta}{dt^2} + \frac{g}{L} \sin \theta = 0 \quad (10)$$

where  $\theta$  is the angular displacement,  $t$  is the time,  $g$  is the acceleration due to gravity and  $L$  is the length of the pendulum [5]. To solve this nonlinear equation, consider that the oscillations of the pendulum are subjected to the initial conditions

$$\theta(0) = \theta_0 \quad \text{and} \quad \left(\frac{d\theta}{dt}\right)_{t=0} = 0 \quad (11)$$

where  $\theta_0$  is the amplitude or the maximum angular displacement at time zero measured from the vertical line. An exact analytical solution for the period in terms of an elliptic integral is given by

$$T = 4 \sqrt{\frac{L}{g}} \int_0^{\frac{\pi}{2}} \frac{d\psi}{\sqrt{1 - \kappa^2 \sin^2 \psi}} = 4 \sqrt{\frac{L}{g}} F\left(\frac{\pi}{2}, \kappa\right) = 4 \sqrt{\frac{L}{g}} K(\kappa). \quad (12)$$

Here  $K(\kappa)$  is a complete elliptic integral of first kind with  $\kappa^2 = \frac{L\omega_0^2}{4g} < 1$  and  $\omega_0$  is the angular velocity. If the arm is not massless, the pendulum's period depends on its moment of inertia and is given in [6] by:

$$T = 4 \sqrt{\frac{I_{CM} + ml^2}{mgl}} \int_0^{\frac{\pi}{2}} \frac{d\psi}{\sqrt{1 - \kappa^2 \sin^2 \psi}} \quad (13)$$

where  $I_{CM}$  represents the mass moment of inertia with respect to the mass center of the pendulum and  $l$  denotes the length of the pendulum from the hung point to the mass center of the pendulum. The angular displacement  $\theta$  as a function of  $t$  can be represented using the expression:

$$\theta(t) = 2 \sin^{-1} \left\{ \sin \frac{\theta_0}{2} \operatorname{sn}[K(\kappa) - \omega t; \kappa] \right\} \quad (14)$$

where  $\operatorname{sn}$  represents the Jacobi elliptic function and  $\omega = \frac{2\pi}{T_0}$  denotes the angular frequency [7]. The reaction force can be calculated according to [6] by:

$$F = m \frac{v^2}{L} + mg \cos \theta. \quad (15)$$

Here, the velocity  $v$  is calculated from the equation

$$v = L \frac{d\theta}{dt} = L \sqrt{\frac{2g}{L}} \sqrt{(\cos \theta - \cos \theta_0)} \quad (16)$$

where  $\frac{d\theta}{dt}$  is obtained from the integration of Eq. 10.

#### 4 IGA implementation in LS-DYNA for test case

A practical example of the pendulum is developed in LS-PrePost for illustrating the stepwise description of the implementation procedure. In this example, the effect of contact surface smoothness is analyzed by employing various contact types.

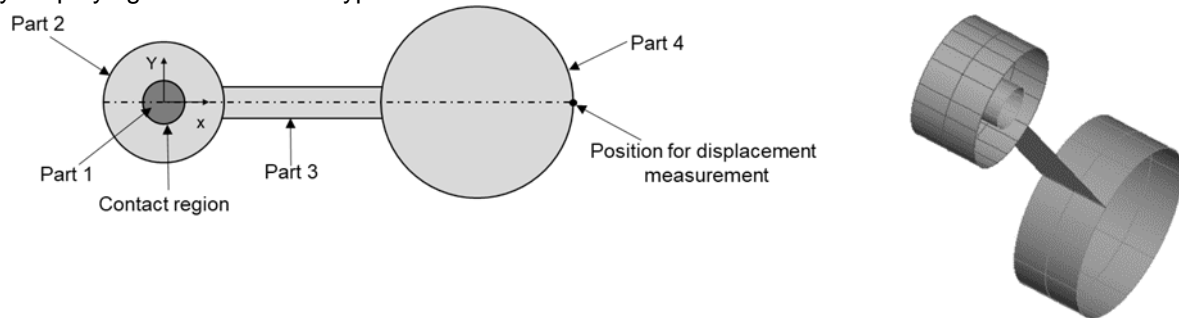


Fig.2: Pendulum under gravity load (left) and NURBS model of the pendulum (right).

##### 4.1 Construction of NURBS discretized geometry and boundary conditions

In IGA, conversion of CAD model to NURBS patches requires parametric details such as control points, order of NURBS basis functions and knot vectors. In LS-PrePost NURBS patches are created from CAD geometry and the necessary geometric information including control points in local r- and s- direction, order of basis functions and knot vectors in both direction are automatically generated. These NURBS patches can be modified further by using various refinement options without altering the original geometry. For the given example of the pendulum, the inner part (part 1) is divided into two Nurbs patches, while the remaining part of the pendulum consists of five Nurbs patches. In this case, quadratic NURBS basis functions are used to construct the NURBS discretized geometry. The continuity of the NURBS basis functions at the junction between different patches dropped from  $C^1$  to  $C^0$ . In Fig. 3 quadratic NURBS basis function profiles are plotted for part 1 and it can be observed that inter element continuity of the basis function is  $C^1$  which is dropped to  $C^0$  where the knots are repeated and also at the junction of NURBS patches.

knot vector for NURBS patch

$$\xi = \left\{ 0, 0, 0, \frac{1}{4}, \frac{1}{2}, \frac{1}{2}, \frac{3}{4}, 1, 1, 1 \right\}$$

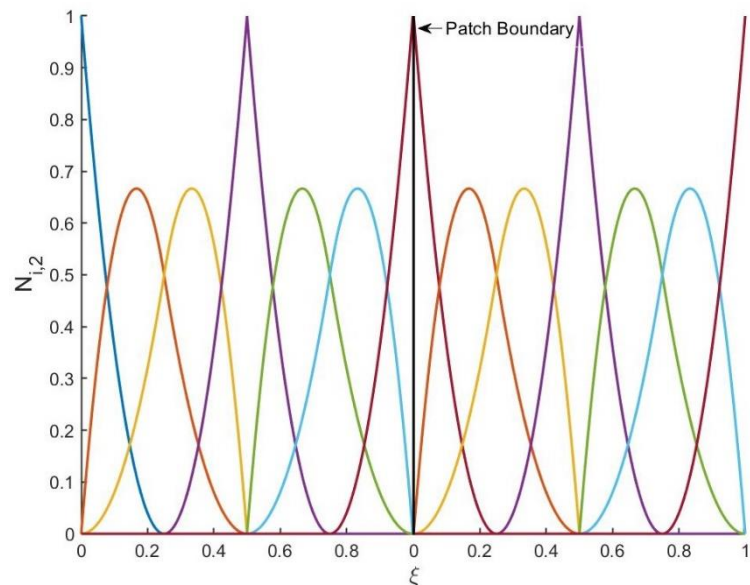


Fig.3: Quadratic NURBS basis function profiles for part 1.

For the purpose of comparison, three different cases based on biquadratic NURBS elements and three cases using standard bilinear shell elements are considered and their details for each part is presented

in table 1, while inner and outer part of the pendulum under different NURBS discretizations are shown in Fig. 4.

Parts	Case (Biquadratic Nurbs element)			Case (Bilinear Shell element)		
	I	II	III	I	II	III
1	4x1	8x2	12x3	12x6	18x9	32x17
2	8x1	20x2	44x3	32x6	50x9	88x17
3	5x1	6x2	7x3	23x6	36x9	66x17
4	8x1	10x2	12x3	46x6	70x9	126x17

Table 1: Detail of NURBS and standard shell elements.

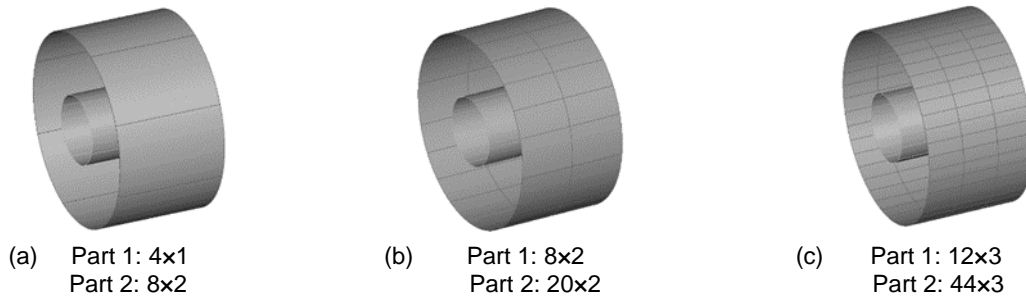


Fig.4: Biquadratic NURBS elements.

According to the specific case of the pendulum the inner part (part 1) is fixed while the remaining part of the pendulum may rotate freely under gravity load. Linear elastic mild steel properties are used for the given example. Frictionless contact is defined between part 1 and part 2 and the gravity load is applied using the keyword **\*LOAD\_BODY\_ (OPTION)**. The one way contact interface **\*AUTOMATIC\_ONE\_WAY\_SURFACE\_TO\_SURFACE** and **\*AUTOMATIC\_SURFACE\_TO\_SURFACE** contacts are used for this study. In one-way contact, only the slave side is checked for penetration against the master segments while the master nodes do not undergo any sort of checking. On the contrary, surface to surface contact is identical to one-way except the penetration detection is symmetric. In this type, first the nodes of the slave segments are checked for a possible penetration against the master segments after which the master nodes are checked against the slave segments. In LS-DYNA two possibilities are available for contact boundary conditions of NURBS-based finite elements. The first possibility is that the geometry of the contacting NURBS surfaces can be approximated using bilinear quadrilateral interpolation elements so that the existing FEM contact formulations are immediately accessible. These interpolation elements do not play any role in the actual computation and thus their contribution to the stiffness of the shell is zero. In the second possible case, the actual NURBS surface can be used as the master surface in the contact formulation and interpolation nodes on the slave surface are projected onto the master surface which is defined by the NURBS basis functions. This can be implemented by activating **IGACTC=1** in **\*CONTROL\_CONTACT**. By this, the master surface of the pendulum is represented by a real smooth NURBS surface instead of bilinear quadrilateral interpolation elements. On the other hand, the master surface defined by the standard shell elements is replaced by a smooth curve fitted surface in case of classical FEM. Reissner-Mindlin theory with **ELFORM=16** for FEA and **FORM=0** for IGA are chosen for modeling this problem. Reissner-Mindlin theory is applied because it requires only  $C^0$  continuity and in this example inter element continuity is not purely  $C^1$  but it dropped to  $C^0$  at the junction of the NURBS patch. The y-coordinate of the outermost node of the pendulum (position of the outer node used for measurement is mentioned in Fig. 2) and the overall contact force at the interface from the penalty based contacts are recorded for different contact types for the purpose of comparison.

## 4.2 Results and discussion

The result from the penalty-based contacts of case I predicted by classical FEM is plotted in Fig. 5. It is evident from the figure that the contact type adopting the faceted representation of the master surface using standard shell elements locks the pendulum to the inner part (green curve). It is possible to allow the rotation of the pendulum by modifying the default setting on **\*CONTROL** and **\*CONTACT** card. For example, reducing the penalty stiffness factor (SLSFAC on the **\*CONTROL\_CONTACT** card) from 0.1 to 0.001 allows the relative motion of the pendulum. All other values including the viscous damping coefficient (VDC) remain unchanged. The reduction in contact stiffness factor to 0.001 yields the

penetration of the master nodes into the slave body which is of questionable value. Another remedy that can be used to obtain the desired rotation of the pendulum is to decrease the diameter of the part 1 artificially by a small amount (see Fig.6).

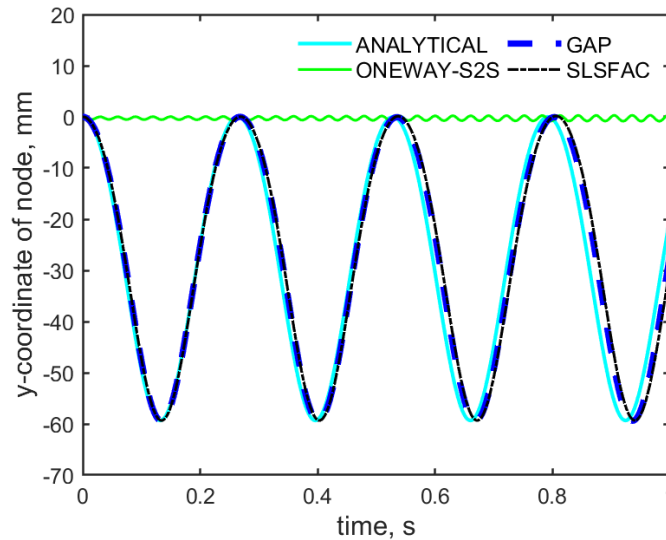


Fig.5: Y-coordinate of the outermost node of the pendulum for classical FE model (case I).

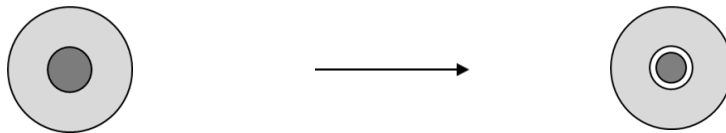


Fig.6: Original configuration (left) and gap provided between parts (right).

However, if the master surface of standard shell elements is replaced by the smooth curve surface by employing the **\*CONTACT ... SMOOTH** algorithm then the desired rotation can be achieved without modifying the original geometry or the default setting on the **\*CONTROL** and **\*CONTACT** card. In case of IGA, the master surface defined by the smooth NURBS surfaces immediately gives the desired rotation of the pendulum. Both, the contact surfaces that use smooth curve surfaces and NURBS surfaces give the desired result despite that a coarser mesh is employed for case I (mesh detail can be seen in table 1).

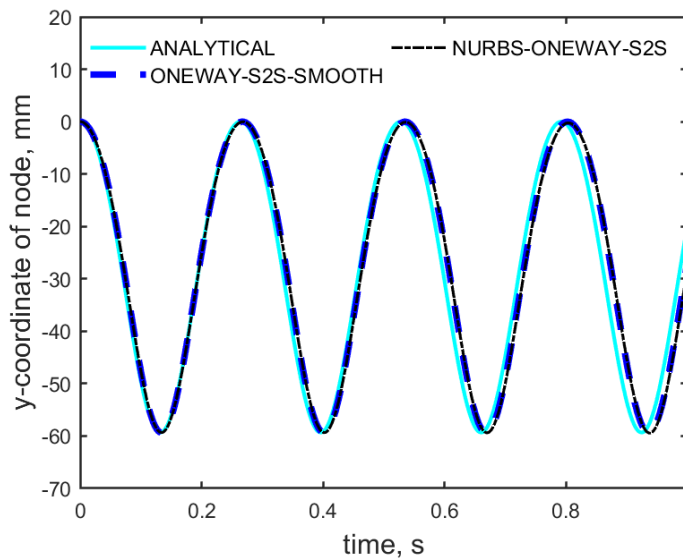


Fig.7: Y-coordinate of the outermost node of the pendulum for NURBS model and smoothed classical FE model (case I).

The analytical solution for the rotation of the pendulum is calculated according to Eq. 13 and Eq.14. Fig. 7 shows that simulation results are in good agreement with the analytical solution. The period of the pendulum evaluated analytically is about 0.524 s which is deviated to 0.535 s in case of the numerical simulation. The contact forces, obtained using different approaches, are presented in Fig. 8 for faceted and NURBS surfaces. The non-physical oscillations in the contact forces can be observed for the faceted contact description. In fact, adopting the **\*CONTACT\_...\_SMOOTH** option also gives spurious oscillation in the contact force, while the amplitude of the contact force oscillation is significantly less as compared to the approach where an artificial gap is provided between two contact surfaces. On the other hand, smoothing the master surface by the NURBS surface effectively alleviates the contact force oscillation to great extent.

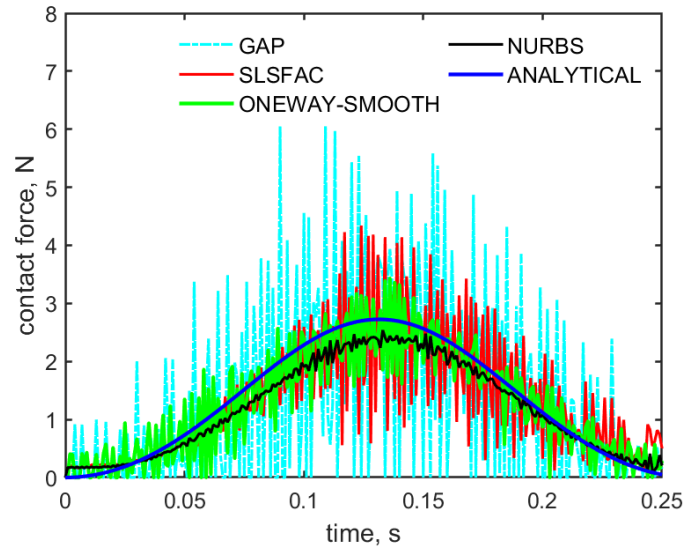


Fig.8: Comparison of contact force oscillations for case I.

Initially, the mesh was intentionally constructed with large size elements in order to demonstrate the fact that NURBS surfaces combat with the mesh interlocking problem without providing any additional smoothing strategy. For case II, the mesh refinement is more typical and improves the results of the simulation but the rotation of the pendulum still contains some period errors using default settings. The result for the case II in Fig. 9 indicates that standard shell elements using a smooth contact algorithm and NURBS surfaces in case of IGA work perfectly. However, the definition of the non-smooth contacts is still not able to produce the desired result.

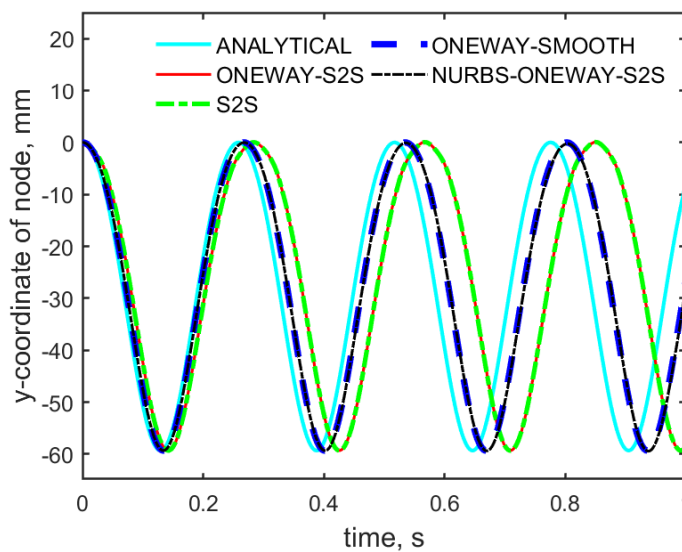


Fig.9: Y-coordinate of the outermost node of the pendulum for case II.

In the case III, mesh refinement using standard shell elements improves the result, as expected and one gets the desired rotation of the pendulum for non-smooth contacts too (see Fig. 10). This means that a compatible mesh is always required at the interface to get the desired output but this difficulty can be overcome by defining the smooth contact algorithm in case of classical FEM or smooth NURBS surfaces in case of IGA.

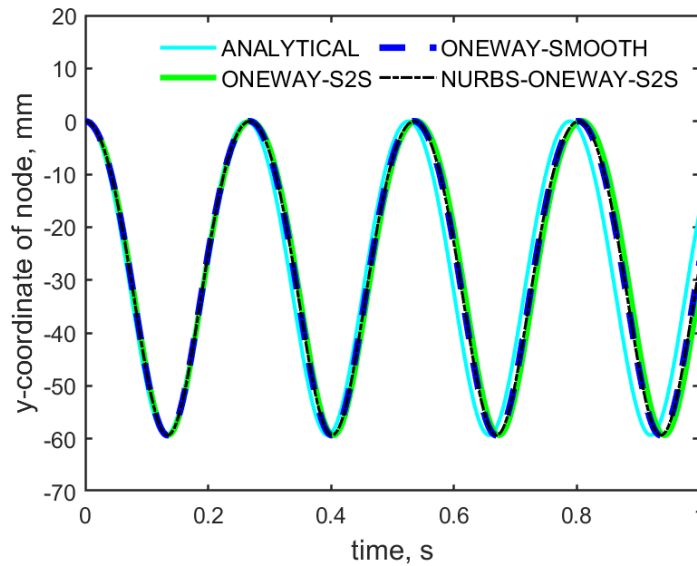


Fig.10: Y-coordinate of the outermost node of the pendulum for case III.

However, the discontinuity of the surface normal vector field induced by the standard shell element contact description still produces the spurious oscillations in the contact force, as shown in Fig. 11.

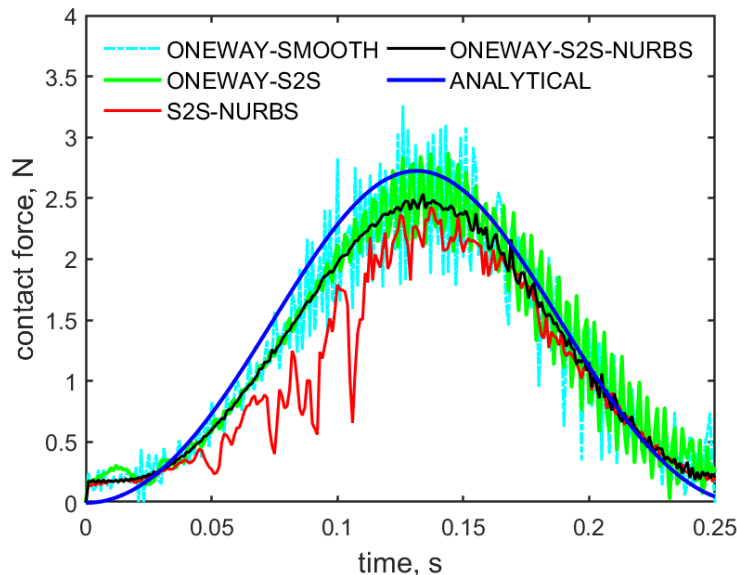


Fig.11: Comparison between faceted and NURBS master surface description for case III.

But the amplitude of the contact force oscillations decreases upon mesh refinement, as expected. On the other hand, smoothing the master surface with a NURBS surface yields insignificant oscillations in the contact force. Here, NURBS surfaces lead to minor artificial oscillations in contact force when **\*AUTOMATIC\_ONEWAY\_SURFACE\_TO\_SURFACE** contact is employed, while **\*AUTOMATIC\_SURFACE\_TO\_SURFACE** contact still shows non-physical oscillations in the contact force. The behavior of these oscillations remains until 0.15 s. After that the amplitude of these oscillations decreases. The influence of the mesh refinement on the contact force can be observed from Fig. 8 and Fig. 11. Further, it can be concluded from the comparison that mesh refinement of NURBS surfaces

does not affect too much the contact force oscillations. These small non-physical oscillations in contact force may be due to the fact that inter element continuity of NURBS surfaces is not purely  $C^1$  but it dropped to  $C^0$  at the repeated knots and at the junction of the NURBS patches. The maximum value of contact force computed analytically is about 2.73 N which is deviated to 2.49 N in case of numerical simulations.

## 5 Numerical example of the cylindrical roller bearing

A more practical example of a bearing with cylindrical rollers is chosen for a further study. To define the adequate accuracy of the bearing, the finite element modeling of the roller bearing requires a large FE model size and related calculation time while an exact model of the bearing can be represented by a smaller number of control points in case of NURBS modeling.

### 5.1 Modeling and boundary conditions

The simple model of the bearing comprises the following components: an inner race, 4 rolling elements (rollers), a cage and an outer race. The dimensions of the inner and outer raceways and rolling elements for the current simulation are as follows: inner race way diameter  $D_i = 20$  mm, outer raceway diameter  $D_o = 47$  mm, rolling element diameter  $D_r = 7.4$  mm, rolling element depth  $l_d = 8$  mm. The inner and outer race and the rollers are modeled with NURBS shell elements while the cage is modeled by beam elements, see Fig.12 (left). A FE shell element model of the rolling element bearing with the aforementioned dimensions is also built for the purpose of comparison. The material properties used are  $E=210$  GPa,  $\rho = 7850$  kg/m<sup>3</sup>, and  $\nu=0.3$ . An elastic material model is chosen for the current simulation. During the operation of a bearing, it is required that the rolling elements should be in proper contact with the outer and inner raceway at all times during the simulation and they should rotate about the axis of the bearing and their own axis due to contact interaction between rotating inner and stationary outer race. A frictional **\*AUTOMATIC\_SURFACE\_TO\_SURFACE** contact with a static frictional coefficient of 0.145 and a dynamic coefficient of 0.115 is applied for the following contact interfaces within the model: inner race-rolling elements and rolling elements-outer race. For that case, **\*AUTOMATIC\_ONEWAY\_SURFACE\_TO\_SURFACE** contact does not represent the real dynamic characteristics of the bearing. All degrees of freedom of the outer race are restricted and for the cage which is modeled using beam elements, X,Y,Z translational degrees of freedom and X,Y rotational degrees of freedom are constrained. A moment is applied to the beam element which is transferred to the inner race using RBE3 elements. The standard gravity load is also applied to the model.

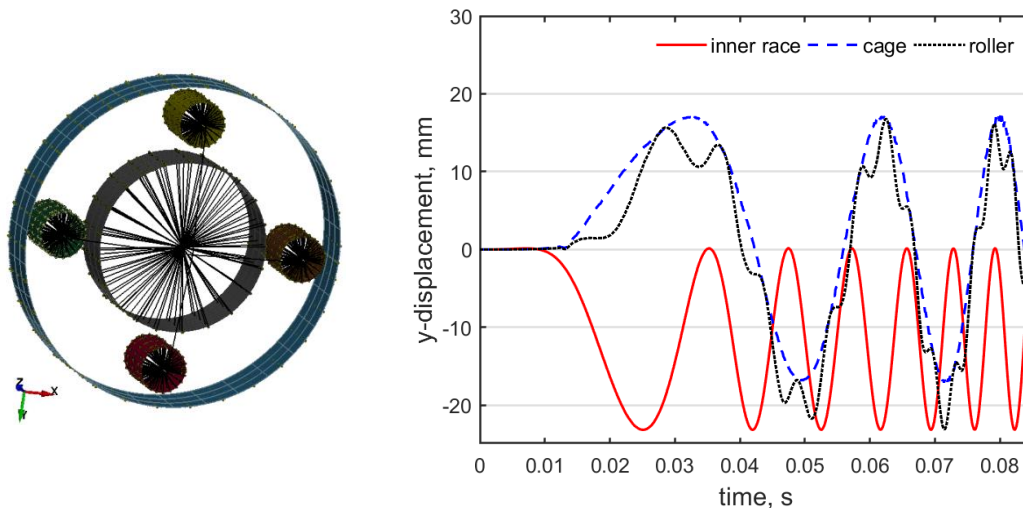


Fig.12: NURBS model of the bearing (left) and y-displacement of nodes in cage and inner and outer race (right).

### 5.2 Results and analysis

It is assumed that relative motion between raceway and rolling element is purely rolling. The dynamic characteristics of the bearing are obtained and it can be seen from Fig. 12 (right) that the rotational speed of the rolling element and the cage are almost the same. The comparison of the contact force between FEM and IGA is presented in Fig.13. This shows the force interaction between outer race and roller and it is clear from the figure that the faceted description of the master surface leads to a strong

oscillation in the resulting contact force. On the other hand, the description of master surface by using smooth NURBS surfaces reduces the oscillation in contact force.

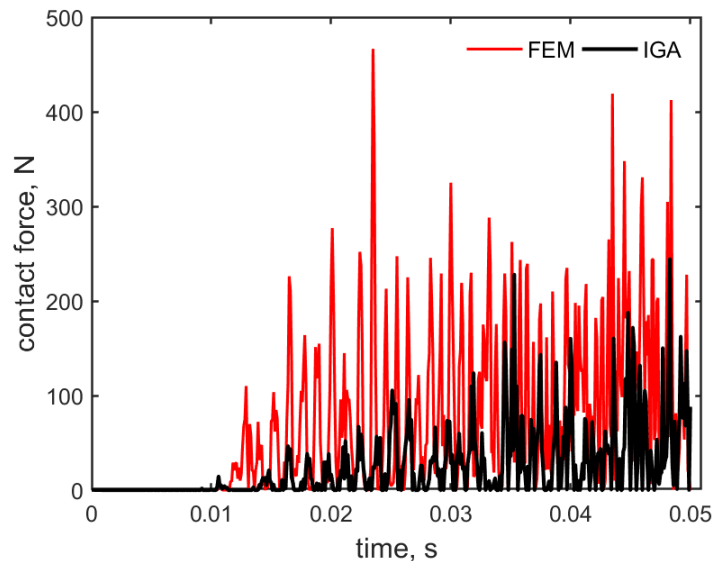


Fig. 13: Force interaction between roller and outer race.

## 6 Summary and conclusion

The pendulum example presented in this paper illustrates how spurious oscillations in contact forces and mesh interlocking problems can be circumvented by using different approaches. The contact surface of coarsely meshed geometry represented by a faceted surface allows rotation of the parts by reducing the penalty stiffness factor but the amount of penetration between contact surfaces becomes questionable. Mesh refinement improves the mesh interlocking and the non-physical oscillations in contact forces but does not completely alleviate the spurious oscillations in the contact force. Smooth contact algorithms in case of FEM show remarkable results of displacements for the given examples, while artificial oscillations are still observed even though smaller elements are adopted for analysis. Non-physical oscillations in contact force show improvement using NURBS surfaces as being demonstrated in numerical examples. On the other hand, **\*AUTOMATIC\_ONEWAY\_SURFACE\_TO\_SURFACE** contact using NURBS surfaces perform remarkably well for the pendulum example only while in case of the bearing it does not represent the real dynamic characteristics of the bearing. Contacting NURBS surfaces approximated using bilinear quadrilateral interpolation elements work quite fine but same surfaces pose issues when described by real NURBS surfaces.

## 7 Acknowledgments

This research was funded by the "Investitionsbank des Landes Brandenburg" with financial resources of the Ministry for Economic Affairs and Energy of the state of Brandenburg and the European Regional Development Fund.

## 8 Literature

- [1] Kopačk, J., Kolman, R.: "Isogeometric contact analysis: A study of an explicit dynamics contact algorithm", 2014
- [2] Lorenzis, L. D., Wriggers, P., and Hughes, T. J. R.: "Isogeometric contact: A review". GAMM Mitteilungen, vol. 37, no. 1, 2014, pp. 85-123
- [3] Cottrell, J. A., Hughes, T. J. R., & Bazilvers, Y.: "Isogeometric analysis: toward integration of CAD FEA", John Wiley & Sons, 2009
- [4] Piegel, L., Tiller, W.: "The NURBS Book", Springer-Verlag, 1995
- [5] Szabo, I.: "Einführung in die Technische Mechanik", Springer-Verlag, 1984, pp. 249-252
- [6] Awrejcewicz, J.: "Classical Mechanics: Dynamics", Springer, 2012
- [7] Beléndez, A., Pascual, C., Méndez D.I., Beléndez, T., Neipp, C.: "Exact solution for the nonlinear pendulum", Revista Brasileira de Ensino de Física, vol. 29, no. 4, 2007, pp. 645-648